The Cryosphere Discuss., 6, 3011–3048, 2012
www.the-cryosphere-discuss.net/6/3011/2012/
doi:10.5194/tcd-6-3011-2012

The Cryosphere Discussions

The impact of heterogeneous surface temperatures on the 2-m air temperature over the Arctic Ocean in spring

A. Tetzlaff[1,2], **L. Kaleschke**[1], **C. Lüpkes**[2], **F. Ament**[3], **and T. Vihma**[4]

[1]Institute of Oceanography, University of Hamburg, Germany
[2]Alfred Wegener Institute for Polar and Marine Research, Bremerhaven, Germany
[3]Institute of Meteorology, University of Hamburg, Germany
[4]Finnish Meteorological Institute, Helsinki, Finland

Received: 3 July 2012 – Accepted: 10 July 2012 – Published: 31 July 2012

Correspondence to: A. Tetzlaff (amelie.tetzlaff@awi.de)

Published by Copernicus Publications on behalf of the European Geosciences Union.

Abstract

The influence of spatial surface temperature changes over the Arctic Ocean on the 2-m air temperature variability is estimated using backward trajectories based on ERA-Interim and the JRA25 wind fields. They are initiated at Alert, Barrow and at the Tara drifting station. Three different methods are used. The first one compares mean ice surface temperatures along the trajectories to the observed 2-m air temperatures at the stations. The second one correlates the observed temperatures to air temperatures obtained using a simple Lagrangian box model which only includes the effect of sensible heat fluxes. For the third method, mean sensible heat fluxes from the model are correlated with the difference of the air temperatures at the model starting point and the observed temperatures at the stations. The calculations are based on MODIS ice surface temperatures and four different sets of ice concentration derived from SSM/I and AMSR-E data. Under nearly cloud free conditions, up to 90 % of the 2-m air temperature variance can be explained for Alert, and 60 % for Barrow using these methods. The differences are attributed to the different ice conditions, which are characterized by high ice concentration around Alert and lower ice concentration near Barrow. These results are robust for the different sets of reanalyses and ice concentration data. Near-surface winds of both reanalyses show a large inconsistency in the Central Arctic, which leads to a large difference in the correlations between modeled and observed 2-m air temperatures at Tara. Explained variances amount to 70 % using JRA and only 45 % using ERA. The results also suggest that near-surface temperatures at a given site are influenced by the variability of surface temperatures in a domain of about 150 to 350 km radius around the site.

1 Introduction

Sea ice plays an important role in the climate system. It insulates the ocean from the atmosphere and thus hampers the exchange of gases, moisture and heat. The strength

TCD
6, 3011–3048, 2012

of the insulation effect depends, however, on the sea ice thickness and sea ice concentration. Openings in sea ice act as windows and allow a direct ocean-atmosphere interaction with a large impact on the surface energy budget of the polar ocean and atmosphere. In order to obtain accurate fluxes, which determine the energy budgets, the sea ice concentration should be well represented in climate and weather prediction models. Also for reanalyses, a correct representation of ice concentrations is crucial for heat flux calculations (Inoue et al., 2011).

In this context the importance of accurate ice concentration measurements becomes apparent. Using remote sensing data from the Special Sensor Microwave Imager (SSM/I), uncertainties of at least 4 % arise for different algorithms in regions with high ice concentrations such as the Central Arctic (Andersen et al., 2007).

Several modeling studies have revealed a high sensitivity of atmospheric boundary layer temperatures to the ice cover. Lüpkes et al. (2008) used a one dimensional atmospheric model coupled with a sea ice model to investigate the influence of a change in ice cover on the atmospheric boundary layer temperatures. They found that, under clear skies in winter and for ice concentrations close to 100 %, a change in ice concentration of 1 % can cause a temperature change of up to 3.5 K. Simmonds and Budd (1990) investigated the effect of a reduced sea ice cover in the Antarctic in a general circulation model. Reducing the ice cover from 100 to 50 % caused an increase of the sensible heat flux over the Southern Hemisphere sea ice zone of 80 Wm^{-2} during July and an increase of the zonal mean temperature of up to 6 °C. Valkonen et al. (2008) have shown that, during a cold-air outbreak in the Antarctic sea ice zone, the modeled 2-m air temperature varied by up to 13 K depending on the algorithm applied to derive the sea ice concentration. Parkinson et al. (2001) found that uncertainties in total ice concentrations of ±7 % can cause local temperature changes exceeding 6 °C in polar regions and changes in global annual mean temperatures of about 0.3 °C using a global climate model.

Leads represent a large source for surface temperature variability. Different characteristics of their impact on the atmospheric boundary layer have been measured, such

TCD
6, 3011–3048, 2012

as the annual cycle of sensible heat fluxes (Persson et al., 1992) and the development of sensible heat fluxes on the downwind side of leads (Ruffieux et al., 1995) or different convection regimes over leads (Andreas and Cash, 1999). Heat fluxes over ice and open water areas have also been obtained from aircraft measurements (Fiedler et al., 2010) and have been estimated using surface temperatures from the Advanced Very High Resolution Radiometer (AVHRR) (Meier et al., 1997; Overland et al., 2000). Heat and moisture fluxes from polynyas have been estimated using data from the Special Sensor Microwave Imager (SSM/I) (Martin et al., 2004) and the Advanced Microwave Scanning Radiometer for EOS (AMSR-E) (Boisvert et al., 2012).

The goal of the present study is to supplement the above mentioned studies on the impact of sea ice variability by studying the impact of spatial surface temperature variability on the air temperature at a given location. For this purpose, backward trajectories arriving at three stations in the Arctic are calculated from reanalysis data. Ice concentrations and ice surface temperatures along the trajectories are prescribed from satellite data. The mean ice surface temperature along the trajectories, as well as the air temperature and sensible heat fluxes obtained by a simple Lagrangian box model are then compared to the 2-m air temperatures measured at the stations.

The application of these methods aims to obtain answers to the following questions: How important are spatial changes in surface temperatures in the high ice concentration regime in order to explain atmospheric temperature changes? To what spatial extent do heterogeneous surface temperatures influence the air temperature variability? How strong do the results depend on the choice of different reanalyses for the calculation of trajectories and on different sea ice concentration products?

A description of the data is given in Sect. 2 and the methods are described in Sect. 3. The results are presented in Sect. 4, followed by a discussion (Sect. 5) and conclusions (Sect. 6).

TCD
6, 3011–3048, 2012

2 Data

For the present study, hourly 2-m air temperatures from three different stations in the Arctic are used. These stations are Barrow (Alaska), Alert (Canada) and the French schooner Tara (Fig. 1). The latter drifted through the Central Arctic in 2007 during a campaign which was part of the project DAMOCLES (Developing Arctic Modeling and Observing Capabilities for Long-term Environmental Studies) (Vihma et al., 2008). Only the coldest months with the largest ice extent are used. For the present analysis, these are February and March for Barrow (2003–2008), February through April for Alert (2003–2006) and April 2007 for Tara.

Backward-trajectories arriving at the stations are calculated from the surface wind fields of the Japanese 25-yr reanalysis (JRA) (Onogi et al., 2007) and from the 10 m-wind fields of the European Centre for Medium-Range Weather Forecasts (ECMWF) reanalysis (ERA-Interim) (Dee et al., 2011). JRA has a resolution of 1.125° and ERA of 1.5° (and 0.75°), both are available every 6 h. Sea level pressure fields from both reanalyses are used to calculate potential temperatures. The ERA forecast runs also provide boundary layer depths every 3 h.

The Lagrangian box model following the trajectories requires ice concentration and ice surface temperature as input data. Four different ice concentration data sets are used. These are the Special Sensor Microwave Imager (SSM/I) data with a resolution of 12.5 km (Kaleschke et al., 2001) and AMSR-E with a resolution of 6.25 km (Spreen et al., 2008) starting in June 2002. Both ice concentrations are derived using the ARTIST sea ice (ASI) algorithm (Kaleschke et al., 2001) and are available through the CliSAP-Integrated Climate Data Center (ICDC). In addition, ice concentrations from AMSR-E using the NASA Team 2 (NT2) and the Bootstrap algorithm are used (Cavalieri et al., 2004). Both have a grid spacing of 12.5 km and are provided by NSIDC. Abbreviations for the different combinations of reanalyses and ice concentration data are given in Table 1 and are labeled as a sequence of reanalysis, sensor and algorithm.

TCD
6, 3011–3048, 2012

Sea ice surface temperatures are obtained from the MOD29 (MODIS/Terra Sea Ice Extent and IST Daily L3 Global 4 km EASE-Grid Day) data set by Hall et al. (2006). Data have been available since 24 February 2000 with a resolution of 4 km. They are aggregated to a 12.5 km grid. MOD29 data contain gaps, mainly due to clouds. Considering all trajectories over ice, there are 8 % missing values for Barrow, 20 % for Alert and 32 % for Tara. Since positive cloud radiative forcing changes ice surface temperatures considerably, only nearly cloud free trajectories with less than 10 % missing values are considered. Here, the missing values are replaced using a linear interpolation along the trajectory.

3 Methods

3.1 Backward-trajectories

Two-dimensional trajectories are calculated based on the surface wind fields of the JRA and ERA reanalyses. A time step of 1 h is used for the calculation and the velocity at a certain point is obtained by linearly weighting the wind velocities of the surrounding four points according to their distance in spherical coordinates. Only those trajectories are considered, which do not pass over land along their path.

3.2 Statistical analysis method

The influence of surface temperatures along the trajectories on atmospheric boundary layer temperatures is examined using three different methods. As a first approach, the mean ice surface temperatures along the trajectories are compared to the in situ 2-m air temperatures at the stations (IST method) by calculating correlation coefficients r, root mean squared errors (RMSE) and biases. This approach does not account for the impact of the spatial surface temperature variability along one trajectory. However, the spatial variability of the ice surface temperatures between trajectories with different paths is regarded. Since the MOD29 ice surface temperatures are given as daily fields,

TCD
6, 3011–3048, 2012

the observed variability during one day is only due to spatial differences caused by different trajectory paths and not due to temporal changes of the ice surface temperature. For time periods longer than one day, there is also the day-to-day variability of the ice surface temperatures. It can be shown by a simple statistical analysis that the impact of this variability on correlation coefficients is small compared with the spatial variability caused by different trajectory paths.

The second approach includes the influence of the spatial surface temperature variability along each trajectory by its impact on the air temperature evolution along the trajectories which is calculated using a simple box model (Sect. 3.3). In the following, this method is called the air temperature method (AT). Air temperature changes are only caused by sensible heat fluxes from ice or open water areas in the model. Therefore, the squared correlation coefficient between the modeled and the observed 2-m air temperature at the stations gives the amount of air temperature variability which is explained by changes in surface sensible heat fluxes. The spatial extent at which surface temperature changes are important for air temperature variability is then the radius of impact. It is determined by analyzing the changes of the explained variances as a function of the trajectory length.

Another possibility to get information about the radius of impact can be based on the investigation of the temperature changes along trajectories caused by heat fluxes. In this third approach, the differences between the observed temperatures at the trajectory starting and ending points (the latter are Barrow, Alert and Tara) are correlated with the mean sensible heat fluxes along the trajectories. As a first guess, the air temperature at the trajectory starting point is assumed to equal the ice surface temperature. In the following, this method is called the temperature variability method (TV). The sensible heat fluxes are obtained from the same simple box model as used for the AT method. Results of IST and AT are presented in Sect. 4.4 while TV results are added in Sect. 4.5 only.

For all methods, 95 % confidence intervals for the correlations are obtained using a Fisher's z-transformation (von Storch and Zwiers, 1999). In addition, biases and

TCD
6, 3011–3048, 2012

RMSE between the temperatures are calculated. The significance of these values can be tested using a student-t test (von Storch and Zwiers, 1999). These significance tests require the degrees of freedom. Since hourly temperature measurements are not statistically independent, the degrees of freedom are not equal to the number of observations. Therefore, lag correlations of the in situ temperatures are calculated. The time, where the 95 % confidence interval of the lag correlation reaches 1/e, gives the time scale at which observations become independent. These are 27 h for Barrow, 23 h for Alert and 10 h for Tara. The length of the time series is reduced to the effective length and the degrees of freedom are reduced using these time scales.

3.3 Box model

For the AT and TV methods, a simple box model is used to investigate the Lagrangian change of air temperatures along trajectories. The dominant source term in the prognostic equation for potential temperature is assumed to be the turbulent sensible heat flux at the surface. Contributions from other processes such as condensation or radiation are only indirectly taken into account by their impact on the surface temperature which is prescribed from observations. The Lagrangian model considers a box with constant depth H representing the atmospheric boundary layer (BL). The box travels along a trajectory calculated from reanalysis data (Sect. 3.1). For simplification, the BL is assumed to be well mixed with a constant potential temperature above a reference height of 10 m. Below 10 m, a constant flux layer is assumed with logarithmic profiles of wind and potential temperature.

The fluxes of sensible heat over ice and water are weighted with the ice concentration so that the temperature evolution is calculated as

$$H\frac{\mathrm{d}\theta_\mathrm{a}}{\mathrm{d}t} = A|\boldsymbol{u}|C_\mathrm{si}(\theta_\mathrm{i}-\theta_\mathrm{a}) + (1-A)|\boldsymbol{u}|C_\mathrm{sw}(\theta_\mathrm{w}-\theta_\mathrm{a}), \quad (1)$$

where θ_i, θ_w and θ_a are the potential temperatures of ice, water and air, respectively. A is the ice concentration and $|\boldsymbol{u}|$ is the wind speed. The solution of Eq. (1) is based

TCD
6, 3011–3048, 2012

on an explicit Eulerian numerical scheme with a relatively large time step Δt of 15 min. However, for moderate wind speeds a reduction to 1 min caused changes in the order of 0.2 °C only, so that this impact is negligible compared to other uncertainties. The water temperature T_w is permanently at the freezing point of −1.9 °C. C_{si} and C_{sw} are the heat transfer coefficients for ice and water, respectively. They are calculated using the Monin-Obukhov similarity theory as

$$C_s = \frac{\kappa^2}{(\ln(\frac{z}{z_0}) - \Psi_m(\frac{z}{L}))(\ln(\frac{z}{z_T}) - \Psi_h(\frac{z}{L}))}, \quad (2)$$

where L is the Obukhov length, κ the von Kármán constant and the Ψ-functions for momentum and heat are chosen according to Dyer and Hicks (1970). The surface roughness lengths z_0 are assumed to be constant with values of 1 mm for ice and 0.1 mm for water (as often used, for example by Lüpkes et al., 2008) and the roughness lengths for heat z_T are one tenth of it, respectively. L is calculated iteratively using

$$L = \frac{u_*^2 \bar{\theta}}{\kappa g \theta_*} \quad (3)$$

which neglects the influence of humidity. It is inserted into the turbulent scaling parameters for temperature and velocity

$$\theta_* = \kappa(\theta(z) - \theta_s)(\ln(\frac{z}{z_0}) - \Psi_h(\frac{z}{L}))^{-1} \quad (4)$$

$$u_* = \kappa|\boldsymbol{u}|(\ln(\frac{z}{z_0}) - \Psi_m(\frac{z}{L}))^{-1} \quad (5)$$

after Pielke (2002) which are then used to obtain new values of L. $\bar{\theta}$ is the mean potential temperature of the air. Mahrt (1998) have shown that in very stable cases C_s becomes nearly constant. Therefore, an upper limit is set at $\frac{z}{L} = 1$ and constant values of $C_s = 0.68 \times 10^{-3}$ over ice are used for this limit.

TCD
6, 3011–3048, 2012

The transfer coefficients are calculated for a reference height of $z = 10$ m. For comparison with the in situ 2-m air temperatures the potential temperatures are reduced to a height of 2 m, assuming a logarithmic temperature profile below 10 m. Air temperatures are then obtained from the 2-m potential temperatures using the sea level pressure from the reanalysis.

Two different approaches are used for the boundary layer depth. In the first approach it is set to a constant value. Two different values are applied which are typical for the Arctic BL (Lüpkes et al., 2012). The first one, 350 m, was, for example, measured over a flaw lead polynya in the Canadian Archipelago by Raddatz et al. (2011). The second one, 100 m, is close to often observed values (reported e.g. by Tjernström and Graversen, 2009 for the SHEBA project north of Alaska, by Hartmann et al., 1997 for the marginal ice zone or by Lüpkes et al., 2010 for the inner Arctic Ocean). Using larger BL depths would increase the e-folding time (see below) and the model output temperatures would not differ much from the initial temperatures. There were also more than 25 % surface-based inversions in February and March during SHEBA. However, during the cold seasons, leads and polynyas that are passed by the trajectories cause vertical mixing due to convection and thus a deepening of the boundary layer. Therefore, no constant BL depth smaller than 100 m is used.

As a second approach, BL depths are taken from the ERA Interim 3-hourly forecast runs. Values from the four closest points are linearly interpolated to the trajectory positions. A growing BL may cause a downward heat flux from the inversion layer. The sensitivity to this entrainment through the capping temperature inversion has also been tested by using a simple approach relating entrainment to the surface heat fluxes but was found to be negligible relative to other restrictive assumptions.

The initial air temperature is set equal to the ice surface temperature at the trajectory starting point. The impact of this simplified assumption is small when the model is run long enough to reach an equilibrium state. An estimation of the necessary trajectory length can be derived from the e-folding time which can be obtained analytically by

TCD
6, 3011–3048, 2012

using constant transfer coefficients. The solution of Eq. (1) leads to

$$t_e = \frac{H}{|\boldsymbol{u}|(A \cdot C_{\mathrm{si}} + (1 - A) \cdot C_{\mathrm{sw}})}. \quad (6)$$

t_e is a function of the boundary layer depth H, the wind speed $|\boldsymbol{u}|$ and the ice concentration A. To estimate a maximum e-folding time, a wind speed of $5\,\mathrm{m\,s^{-1}}$, an ice concentration of 95 % and a BL depth of 350 m are assumed. The turbulent transfer coefficients are calculated assuming constant potential temperatures of −20 °C for air and −25 °C for ice. This gives an e-folding time of 27 h, corresponding to 480 km length. Therefore, the trajectory length should be larger than 27 h to ensure that the initial conditions have a small impact. However, in most considered cases, the e-folding time is much smaller and already after 2 h the modeled temperature only differs by 0.5 °C from the equilibrium temperature. Nevertheless, the development along trajectories of 30 h is considered.

4 Results

4.1 Trajectory positions

The trajectories calculated using the different reanalyses show large inconsistencies (Fig. 2). They are compared by calculating the mean spatial distances between JRA and ERA (1.5°) trajectories which differ for the three stations. While Barrow and Alert have mean separations in the order of 100 km after 15 h and of 250 km after 30 h, the mean separations for Tara are as large as 350 km after 15 h and 750 km after 30 h. This shows a large inconsistency of the near-surface wind fields of the reanalyses over Arctic sea ice, especially in the Central Arctic. The large uncertainties in the trajectory positions cause large uncertainties in the estimation of the impact of remote areas but in the near environment of about 100 km the uncertainties are much smaller.

TCD
6, 3011–3048, 2012

Comparing ERA Interim trajectories using resolution of 0.75 and 1.5° reveals only small mean separations of less than 20 km after 30 h. Figure 2 also illustrates that using a higher resolution hardly changes the positions of ERA trajectories. Therefore, the lower resolution is used for the following calculations.

4.2 An example of evolution along a single trajectory

Firstly, an example is presented showing the development of the air temperature and sensible heat fluxes obtained using the box model along an individual trajectory. It is the trajectory arriving at Tara on 20 April 2007 at 00:00 UTC (Fig. 3), which has AMSR-E ASI ice concentrations between 80 and 98 % along the path. The air parcel moves about 800 km northward in 30 h. The ice surface temperature varies between −19 and −12 °C (Fig. 4). The sensible heat fluxes do not exceed 150 Wm^{-2} over water because air-sea temperature differences are 17 °C at maximum and the wind speed does not exceed 6 ms^{-1}. The resulting net heat flux is positive but mostly smaller than 40 Wm^{-2}. The largest heat fluxes occur at $t = -25$ h. These fluxes cause an increase of the air temperature by 3 °C. Along the whole trajectory, the potential temperature at 10 m height increases and reaches −12.5 °C at Tara.

4.3 Ice concentration along all trajectories

In the following, the geographical locations of the trajectories and the corresponding ice conditions are examined to obtain a basis for further discussions of differences between the stations. Abbreviations for ice concentrations used in this section are according to Table 1 but without the prefix for the reanalysis. The frequency distributions of ice concentrations along the trajectories are very similar using ERA or JRA. Therefore, the distributions for both reanalyses are combined in Fig. 5.

Most trajectories arriving at Alert originate from the Central Arctic north of Greenland (Fig. 1) where high ice concentrations are present due to convergent ice drift. Comparing the distribution of ice concentrations along all trajectories, shows that more than

TCD
6, 3011–3048, 2012

95 % of the time ice concentrations are 98 % or higher for the three AMSR-E data sets (Fig. 5). SSM/I ASI has a heavier tail with about 30 % of the values between 90 and 98 %. Barrow's trajectories originate from the Beaufort Sea (Fig. 1) where divergences in the Beaufort Gyre decrease the ice concentration. The frequency distribution also reveals lower ice concentrations than for Alert (Fig. 5) with a total of 10 % (AA) up to 50 % (SA) below 98 %.

The considered trajectories arriving at Tara originate from the Central Arctic and the Laptev Sea (Fig. 1). Ice concentrations show a larger variability and lower values than for Alert and Barrow. During 75 % of the time, the ice concentration values are below 95 % for SA. The difference between the ice concentration data sets is largest for Tara with 40 % of the total ice concentrations below 97 % for AA, 25 % below 97 % for AB and almost 100 % above 97 % for AN. While AB and AN show only small changes in the frequency distributions of ice concentration for the three stations, SA and AA show the highest ice concentrations for Alert and the lowest ones for Tara.

4.4 Results for the ensemble of trajectories

The correlation between the observed 2-m air temperatures and the mean ice surface temperatures along the trajectories (IST) and modeled temperatures (AT) is positive and significant at the 95 % level for all combinations of reanalyses, ice concentration data sets and BL depths. The results of the AT method obtained with different ice concentrations show differences in the order of 1 to 5 % but overlapping confidence intervals. Therefore, only exemplary results are presented. The results for AN and AB are almost identical and therefore, only AN is discussed.

Using the AT method, the highest explained variances of almost 90 % are found for Alert. There, the scatter plot shows a good agreement between model and in situ temperatures for EAA (Fig. 6). For ERA, explained variances are about 4 % higher than for JRA (Fig. 7). Using different BL depths has the largest effect on the bias which is about −1 °C for 350 m and does not differ significantly from zero for 100 m and for ERA derived BL depths. RMSE range between 2.5 and 3 °C. The sensitivity of the results

TCD
6, 3011–3048, 2012

to different ice concentration data sets is very small. The explained variance based on the IST method is 86 % using ERA, which is the same order as the model results, and 75 % using JRA, which is about 10 % smaller. Biases and RMSE using the IST method are larger than those from the AT method.

Explained variances for Barrow are smaller than for Alert ranging between 53 and 63 % for the AT method and about 40 % using the IST method (Fig. 7). In all cases, values for a BL depth of 350 m are about 3 % higher than for 100 m and for the run with ERA BL depths. Explained variances using AA are up to 2 % larger than those using the other ice concentrations (not shown). Temperature biases are positive in the order of 1.5 (350 m) to 4 °C (100 m) and the RMSE are about 4 °C. Biases from the IST method are not significantly different from zero.

Tara shows the largest sensitivity to different reanalyses for the AT method. Explained variances are about 70 % using JRA trajectories with RMSE of about 3 °C (Fig. 7). Using ERA trajectories gives smaller explained variances in the order of 45 % with RMSE of about 4 °C. The variance from the IST method for JRA is about 20 % smaller than the explained variance from the AT method. Using ERA trajectories, the variance based on the IST method is in the same order as the explained variance from the AT method but has a bias exceeding −1 °C. All other biases are not significantly different from zero. Explained variances from the AT method are highest using SA but with an RMSE of 4.5 °C (not shown). The results of the other three ice concentrations are similar to each other. For JRA, higher explained variances are obtained using a BL depth of 100 m, whereas explained variances for ERA are higher using 350 m.

In addition, ERA BL depths are compared with the two constant values. The ERA derived BL has the largest thickness (Fig. 8) at Tara. Here, the most frequent value is around 250 m, which is closer to 350 m, but only for the trajectories derived from ERA explained variances using the AT method are larger for a BL of 350 m than for a BL of 100 m. For JRA, a BL of 100 m gives slightly better results. For Barrow, most BL depths can be found around 150 m but the distribution has a tail with some BL depths even exceeding 500 m. This explains why results of the AT method are better for BL depths

TCD
6, 3011–3048, 2012

of 350 m than for 100 m. In Alert, BL depths below 100 m are present in the ERA data and the explained variances are also higher for a BL depth of 100 m. These results are in line with the expected results from the ice concentration distributions. Shallow BLs develop over completely ice covered areas, as observed for Alert, whereas more open water areas, as for Barrow, cause a deepening of the BL.

4.5 Radius of impact

The above analysis does not yet answer the question concerning the dominant horizontal scale R (or the corresponding time scale R_t) influencing the 2-m air temperature. Therefore, in addition to the previous studies, results are considered as a function of the trajectory length which is reduced stepwise from 30 to 2 h. Figure 9 shows results obtained using the AT and the IST methods corresponding to the prescribed trajectory length. Results are exemplarily discussed for JAA, results from ERA differ only slightly.

The clearest results are those for Barrow. There, the explained variances obtained using the AT method are increasing by about 7 % with increasing trajectory length from 2 to 10 h while they remain nearly constant from 10 to 30 h. The corresponding curve based on IST shows a different behavior with a maximum of explained variance for 10 h. Both curves suggest a value R_t = 10 h for the characteristic time scale which corresponds to $R \approx 180$ km since the average wind speed is 5 m s^{-1}. For the IST method the explained variance decreases for distances larger than R or times larger than R_t, because the surface temperatures in remote areas are not any more correlated with the considered location. A similar decrease for the explained variance of the AT method is not seen, because all trajectories starting at time $t > R_t$ pass also the region close to the location with large impact.

Results for biases and RMSE confirm the findings based on the explained variances. For Barrow, biases and RMSE decrease by about 1 °C for trajectory lengths between 2 and 10 h and remain nearly constant for larger lengths. The maximum explained variance from IST coincides with the minimum RMSE from IST, which is smaller than

TCD
6, 3011–3048, 2012

3 °C for a trajectory length of 10 h and increases to almost 8 °C for a trajectory length of 2 h. The bias from IST increases for shorter trajectory lengths from 0 to 5 °C.

Results for Tara with respect to R values are ambiguous. Only biases and RMSE give clear hints. As for Barrow, there is also a decrease of the RMSE and of the absolute value of the bias of about 1 °C for trajectory lengths up to 10 to 20 h in the results of the AT method and those based on IST. However, the explained variance shows only small variability and is even decreasing for $t > 2$ h. It can only be concluded that the R_t is between 2 and 20 h. A possible explanation for this ambiguousness can be seen in the more scattered locations (Fig. 1) of the trajectories compared with Barrow.

For Alert, the results improve only slightly for longer trajectories. Expecting similar results as for Barrow, an impact radius of about 200 km should be detected. However, as can be seen in Fig. 1, most trajectories arriving at Alert start at a distance from Alert smaller than 200 km. Therefore, most of the considered trajectories do not expand beyond the expected radius of impact.

These results are supplemented by explained variances calculated using the TV method (Fig. 10). For Alert and Barrow, the explained variances increase monotonically with increasing trajectory length which shows that heat fluxes in remote areas can have a certain impact on the air temperature at a given location. However, the largest impact in this method is also seen in the first 10 to 20 h where the slope of the curves ist largest. Therefore, a radius of main impact can be defined by relating it to the region with the largest slope of the curves. By this definition, R_t is reached at the transition from steeper to shallower slopes. This transition is pronounced for Barrow at a trajectory length of 10 h which is consistent with the results from the AT method.

For Alert, the explained variances are about 5 to 10 % higher using ERA trajectories than using JRA. The radius of impact is less pronounced, with R_t between 10 and 20 h which corresponds to R between 180 and 350 km. For Tara, there is a less distinct decrease of r^2 using JRA and even an increase using ERA. Nevertheless, the largest increase is found for trajectory lenghts up to 10 h.

TCD
6, 3011–3048, 2012

Correlation length scales for surface air temperatures have also been calculated by Rigor et al. (2000). They correlated 12-hourly temperature data measured at land and ocean stations in the Arctic during 1979 to 1997. In winter, correlations decreased to about 0.8 (corresponding to an explained variance of 0.64) for separations between the stations of 300 to 400 km (their Fig. 5). Thus, despite the different methods used the results agree well with the correlations and the radius of impact found in the present study.

5 Discussion

One can see that the different methods having been applied explain the observed variances in general quite well. However, the RMSE values are as large as 3 to 4 °C. Possible reasons for these large differences of modeled and in situ temperatures are discussed in the following.

5.1 Uncertainties of input data

Comparing trajectory positions calculated from the surface wind fields of the two reanalyses reveals large differences in the order of 100 km after 15 h and even 350 km for Tara. This points to large uncertainties in the surface wind fields. However, inside the main radius of impact, which is only about 10 h, as shown above, the uncertainties in trajectory positions are relatively small.Uncertainties in wind speeds also influence the flux calculations. Taking for example 3 $m\,s^{-1}$ instead of 6 $m\,s^{-1}$ roughly causes a doubling of the fluxes.

Jakobson et al. (2012) compared wind speed profiles from tether-sonde sounding data at Tara to different reanalyses. Using 29 profiles, they found that the ERA and JRA reanalyses generally agree well but slightly overestimate the 10-m wind speeds by about 1 $m\,s^{-1}$ with an RMSE of only 1.5 $m\,s^{-1}$. However, since wind direction data were not available, no comparison was possible for the wind direction which is important for

TCD
6, 3011–3048, 2012

the trajectory positions. Thus, even though ERA reproduced profiles of wind speed, air temperature and humidiy best, JRA might still reproduce the surface wind directions in a better way.

There are also uncertainties in the location of the trajectory points arising from the calculation method. In reality air motions are not only horizontal but air parcels also experience rising or sinking. Since wind speed and direction are usually changing with height, neglecting vertical motions leads to errors in the positions. Thus the representation of an air parcel as a box extending over the entire BL with constant wind represents in most cases only a rough approximation of natural conditions.

Ice concentrations are available only on a daily basis with a grid spacing of 12.5 km (and 6.25 km for AA). This means that small scale features and ice concentration changes on shorter timescales are not captured. Furthermore, there are also uncertainties in the retrieval method. Andersen et al. (2007) compared ice concentrations from SSM/I data using different algorithms to SAR data in winter. They found that the ASI algorithm tends to underestimate ice concentrations close to 100 % by 2.1 % and ice concentrations have an uncertainty range of 3.9 %. NT2 shows a smaller underestimation of 0.4 % similar to Bootstrap with 0.3 % with a larger uncertainty range of 4.9 % in regions with high ice concentrations. A comparison of the algorithms for AMSR-E data in the Arctic show that overall ASI ice concentrations are 1.4 % smaller than Bootstrap and 2.0 % smaller than NT2 ice concentrations (Spreen et al., 2008). Furthermore, Shokr and Kaleschke (2012) showed that ice concentrations are underestimated in the presence of thin ice below 12 cm thickness depending on the surface conditions.

Used ice surface temperatures have up to 10 % missing values, mainly because of clouds. There are also uncertainties concerning the cloud mask and fog is sometimes not classified as clouds (Hall et al., 2006). Furthermore, Hall et al. (2004) compared MODIS ice surface temperatures to in situ measurements and found uncertainties in the order of 1.3 °C. Assuming a constant offset between MOD29 and real ice surface temperatures, however, has the largest effect on the temperature bias but only changes

TCD
6, 3011–3048, 2012

the explained variance by less than 1 %. The large bias of up to 4 °C for Barrow could be caused by a positive bias in MOD29 ice surface temperatures. This can arise, for example, if fog is classified as cloud free and the warmer fog temperature is considered as IST.

Despite these uncertainties the analyses show that spatial surface temperature variability in the environment of a location has a significant impact on 2-m air temperatures at this location. This shows that a good representation of ice concentrations in models would improve not only temperatures but also surface winds since ice concentrations also influence the shape of the wind profile (Tisler et al., 2008) and even the atmospheric pressure patterns.

5.2 Impact of model assumptions

Several model assumptions and simplifications mentioned already in Sect. 3 should also be kept in mind for the interpretation of results obtained by the AT and the TV method. Additional uncertainties which might be responsible for the large RMSE arise, for example, from the used roughness lengths for momentum z_0 and heat z_T which are set constant in the model using the relation $\frac{z_T}{z_0} = 10^{-1}$ for simplicity. For this reason, different constant values of z_0 and z_T over sea ice have been tested but the impact was moderate on both RMSE and biases and the explained variance changed only little. However, it cannot be excluded that variable values accounting for the sea ice topography (Andreas et al., 1984; Garbrecht et al., 1999, 2002; Vihma et al., 2003; Guest and Davidson, 1987; Lüpkes and Birnbaum, 2005; Andreas et al., 2010) would be of a larger impact. This cannot be tested here, because the necessary information about height and distribution of sea ice pressure ridges is not available for the considered regions.

It should also be stressed that the present method does not allow to model the feedback mechanism of the atmospheric processes on sea ice, since ice concentrations and ice surface temperatures are prescribed from satellite data. This implies that,

TCD
6, 3011–3048, 2012

although only sensible heat fluxes occur as a direct source for temperature change in the model equation, also other processes which have contributed to the observed surface temperature variability are indirectly accounted for. Such processes are, for example, heat transport through ice and radiation. A variation of parameters like surface roughness would affect also the surface temperature and sea ice drift but this kind of interaction is also excluded by prescribing the observed surface temperature. This means that the model underestimates the impact of sea ice variability which can only be obtained by a fully coupled ice atmosphere model.

In addition, the ice concentration does only represent the mean ice conditions in one pixel of 12.5 km (or 6.25 km for AA). It does not contain any information about the spatial distribution of open water areas in the pixel area. Andreas and Cash (1999) have shown that the heat transfer from wintertime leads and polynyas is more efficient for small leads. They found transfer coefficients of 1.0×10^{-3} for a fetch larger than 100 m and of 1.8×10^{-3} for smaller fetches. Maslanik and Key (1995) calculated that a fetch increase from 10 to 100 m decrease sensible heat fluxes from an open water lead by 34 %. This means that the spatial distribution, size and orientation of open water areas influence the heat transfer and that our present estimation of open water impact can be seen as a lower limit and the real impact could be much larger (Marcq and Weiss, 2012).

6 Conclusions

The main goal of this study was to investigate the dependence of the 2-m air temperature on the surface temperature variability around three Arctic sites and to determine its characteristic radius of impact. These sites were Alert, Barrow and the French schooner Tara during its drift across the Arctic ocean. Three approaches were used which are based on backward trajectories calculated from surface wind fields of the ERA-Interim and the JRA25 reanalyses. As a first step, the 2-m air temperature measured at the stations was correlated with the average MODIS sea ice surface

TCD
6, 3011–3048, 2012

temperature along the trajectory paths. For the other two methods, a simple Lagrangian box model, which was run along the trajectories, was applied to calculate the surface sensible heat fluxes and the air temperature evolution along the trajectories. Four different ice concentration data sets (SSM/I ASI, AMSR-E ASI, NASA Team 2 and Bootstrap) and MODIS ice surface temperatures were used. For the AT method the modeled temperatures at the stations were compared to the measured ones and for the TV method temperature changes along the trajectories were compared to mean sensible heat fluxes. The investigation was carried out for the cold season with only few clouds to restrict the study to conditions where a large impact of surface fluxes can be expected.

It is found that the AT method explains a large amount, namely 60 to 90 %, of the observed 2-m air temperature variability at all stations when the JRA reanalysis is used, where the number 90 % refers to Alert and 60 % to Barrow. These numbers, which are significant on the 95 % level, are similar for ERA, however, at Tara the explained variance is only about 45 % which might point to problems of ERA with the wind field in the Central Arctic. The results depend only weakly on the sea ice concentration products although they show significant differences in the sea ice distributions. However, in all considered cases it can be seen that those results using AMSR-E ASI ice concentrations are slightly better than those using the NASA Team 2 or Bootstrap ice concentrations. A possible reason for the small impact of ice concentration products might be that the inaccuracy caused by erroneous trajectory positions is masking the inaccuracy of ice concentrations. Another reason is that the prescribed ice surface temperature does not depend on the ice concentration. This would be different in a fully coupled model in which sea ice surface temperature would be adjusted to the modified concentration. Thus it can be concluded that the methods using the present model underestimate the impact of sea ice concentration.

In most considered cases, the IST method explains a smaller percentage of the 2-m air temperature than the AT method but with values ranging still between 40 % and 78 % for Barrow and Alert, respectively. This points to the fact that also the spatial variability

TCD
6, 3011–3048, 2012

rather than only the level of temperature within the range of impact is important. Using ERA trajectories, the model results show no clear improvement for Alert and Tara relative to the results using the mean surface temperatures along the trajectories. This different behavior for the different reanalyses might also be explained by inaccuracies in the trajectory positions.

The characteristic radius of impact of sea ice concentration and surface temperature variability was investigated by varying the trajectory lengths and was found to be between 150 and 350 km assuming an average wind speed of $5\,m\,s^{-1}$. This radius is pronounced for Barrow using all three methods. For Tara, results are ambiguous since only bias and RMSE give a clear dependence on the trajectory length and for Alert, a distinct radius of impact is only found using the TV method.

The present results should be seen in the light of restrictive model assumptions and uncertainties of input data. Nevertheless they reveal a large dependence of atmospheric boundary layer temperatures on heterogeneous surface temperatures in the Arctic which underlines the large importance of a very accurate representation of all processes influencing the surface temperature in climate and weather prediction models.

Acknowledgements. This study was supported through the Cluster of Excellence "CliSAP" (EXC177), University of Hamburg, funded through the German Science Foundation (DFG). A part of this project was also funded by a subproject of MiKlip, a project supported by the German Federal Ministry of Education and Research (FKZ:01LP1126A). The Tara expedition was supported by the European Commission 6th Framework Integrated Project DAMOCLES, and we thank Timo Palo, Erko Jakobson and Jaak Jaagus for providing us with the data. ECMWF ERA-Interim data used in this study have been obtained from the ECMWF data server. JRA reanalysis data used for this study are provided from the cooperative research project of the JRA-25 long-term reanalysis by the Japan Meteorological Agency (JMA) and the Central Research Institute of Electric Power Industry (CRIEPI).

TCD
6, 3011–3048, 2012

References

Andersen, S., Tonboe, R., Kaleschke, L., Heygster, G., and Pedersen, L. T.: Intercomparison of passive microwave sea ice concentration retrievals over the high concentration Arctic sea ice, J. Geophys. Res., 112, C08 004, doi:10.1029/2006JC003543, 2007. 3013, 3028

Andreas, E., Tucker III, W., and Ackley, S. F.: Atmospheric boundary-layer modification, drag coefficient, and surface heat flux in the Antarctic marginal ice zone, J. Geophys. Res., 89, 649–661, doi:10.1029/JC089iC01p00649, 1984. 3029

Andreas, E. L. and Cash, B. A.: Convective heat transfer over wintertime leads and polynyas, J. Geophys. Res., 104, 25721–25734, doi:10.1029/1999JC900241, 1999. 3014, 3030

Andreas, E. L., Persson, P. O. G., Jordan, R. E., Horst, T. W., Guest, P. S., Grachev, A. A., and Fairall, C. W.: Parameterizing turbulent exchange over sea ice in winter, J. Hydromet., 11, 87–104, doi:10.1175/2009JHM1102.1, 2010. 3029

Boisvert, L. N., Markus, T., Parkinson, C. L., and Vihma, T.: Moisture fluxes derived from EOS aqua satellite data for the north water polynya over 2003–2009, J. Geophys. Res., 117, D06 119, doi:10.1029/2011JD016949, 2012. 3014

Cavalieri, D., Markus, T., and Comiso, J.: AMSR-E/Aqua Daily L3 12.5 km Brightness Temperature, Sea Ice Conentration & Snow Depth Polar Grids V002, Boulder, Colorado USA: National Snow and Ice Data Center, 2004. 3015

Dee, D. P., Uppala, S. M., Simmons, A. J., Berrisford, P., Poli, P., Kobayashi, S., Andrae, U., Balmaseda, A., Balsamo, G., Bauer, P., Bechtold, P., Beljaars, A. C. M., van de Berg, L., Bidlot, J., Bormann, N., Delsol, C., Dragani, R., Fuentes, M., Geer, A. J., Haimberger, L., Healy, S. B., Hersbach, H., Holm, E. V., Isaksen, L., Kallberg, P., Köhler, M., Matricardi, M., McNally, A. P., Monge-Sanz, B. M., Morcrette, J., Park, B., Peubey, C., de Rosnay, P., Tavolate, C., Thepaut, J., and Vitart, F.: The ERA-Interim reanalysis: configuration and performance of the data-assimilation system., Q. J. R. Meteorol. Soc., 137, 553–597, doi:10.1002/qj.828, 2011. 3015

Dyer, A. J. and Hicks, B. B.: Flux-gradient relationships in the constant flux layer, Q. J. R. Meteorol. Soc., 96, 715–721, doi:10.1007/s10546-010-9482-3, 1970. 3019

Fiedler, E. K., Lachlan-Cope, T. A., Renfrew, I. A., and King, J. C.: Convective heat transfer over thin ice covered coastal polynyas, J. Geophys. Res., 115, C10051, doi:10.1029/2009JC005797, 2010. 3014

TCD
6, 3011–3048, 2012

Garbrecht, T., Lüpkes, C., Augstein, E., and Wamse, C.: Influence of a sea ice ridge on low-level airflow, J. Geophys. Res., 104, 24499–24507, doi:10.1029/1999JD900488, 1999. 3029
Garbrecht, T., Lüpkes, C., Hartmann, J., and Wolff, M.: Atmospheric drag coefficients over sea ice – validation of a parametrisation concept, Tellus A, 54, 205–219, doi:10.1034/j.1600-0870.2002.01253.x, 2002. 3029
Guest, P. S. and Davidson, K. L.: The effect of observed ice conditions on the drag coefficient in the summer East Greenland sea marginal ice zone, J. Geophys. Res., 92, 6943–6954, doi:10.1029/JC092iC07p06943, 1987. 3029
Hall, D. K., Key, J. R., Casey, K. A., Riggs, G. A., and Cavalieri, D. J.: Sea ice surface temperature product from MODIS, IEEE Trans. Geosc. Rem. Sens., 42, 1076–1087, doi:10.1109/TGRS.2004.825587, 2004. 3028
Hall, D. K., Riggs, G. A., and Salomonson, V. V.: MODIS/Terra Sea Ice Extent and IST Daily L3 Global 4 km EASE-Grid Day V005, Boulder, Colorado USA: National Snow and Ice Data Center, 2006. 3016, 3028
Hartmann, J., Kottmeier, C., and Raasch, R.: Boundary layer development and roll vortex structure during a cold air outbreak, Bound. Layer Met., 84, 45–65, doi:10.1023/A:1000392931768, 1997. 3020
Inoue, J., Masatake, E. H., Enomoto, T., and Kikuchi, T.: Intercomparison of surface heat transfer near the arctic marginal ice zone for multiple reanalyses: a case study of September 2009, SOLA, 7, 57–60, doi:10.2151/sola.2011-015, 2011. 3013
Jakobson, E., Vihma, T., Palo, T., Jakobson, L., Keernik, H., and Jaagus, J.: Validation of atmospheric reanalyses over the Central Arctic Ocean, Geophy. Res. Let., 39, L10 802, doi:10.1029/2012GL051591, 2012. 3027
Kaleschke, L., Heygster, G., Lüpkes, C., Bochert, A., Hartmann, J., Haarpaintner, J., and Vihma, T.: SSM/I sea ice remote sensing for mesoscale ocean-atmosphere interaction analysis, Can. J. Rem. Sens., 27, 526–537, 2001. 3015
Lüpkes, C. and Birnbaum, G.: Surface drag in the Arctic marginal sea-ice zone: a comparison of different parameterisation concepts, Bound. Layer Met., 117, 179–211, doi:10.1007/s10546-005-1445-8, 2005. 3029
Lüpkes, C., Vihma, T., Birnbaum, G., and Wacker, U.: Influence of leads in sea ice on the temperature of the atmospheric boundary layer during polar night, Geophys. Res. Lett., 35, L03 805, doi:10.1029/2007GL032461, 2008. 3013, 3019

TCD
6, 3011–3048, 2012

Lüpkes, C., Vihma, T., Jakobson, E., König-Langlo, G., and Tetzlaff, A.: Meteorological observations from ship cruises during summer to the Central Arctic: a comparison with reanalysis data, Geophys. Res. Lett., 27, L09 810, doi:10.1029/2010GL042724, 2010. 3020

Lüpkes, C., Vihma, T., Birnbaum, G., Dierer, S., Garbrecht, T., Gryanik, V., Gryschka, M., Hartmann, J., Heinemann, G., Kaleschke, L., Raasch, S., and Savijärvi, H., Schlünzen, K., and Wacker, U.: ARCTIC Climate Change - The ACSYS Decade and Beyond, vol. 43 of Atmospheric and Oceanographic Sciences Library, chap. 7. Mesoscale modelling of the Arctic atmospheric boundary layer and its interaction with sea ice, Springer, 2012. 3020

Mahrt, L.: Nocturnal boundary-layer regimes, Bound. Layer Met., 88, 255–278, doi:10.1023/A:1001171313493, 1998. 3019

Marcq, S. and Weiss, J.: Influence of sea ice lead-width distribution on turbulent heat transfer between the ocean and the atmosphere, The Cryosphere, 6, 143–156, doi:10.5194/tc-6-143-2012, 2012. 3030

Martin, S., Drucker, R., Kwok, R., and Holt, B.: Estimation of the thin ice thickness and heat flux for the Chukchi Sea Alaskan coast polynya from Special Sensor Microwave/Imager data, 1990–2001, J. Geophys. Res., 109, C10 012, doi:10.1029/2004JC002428, 2004. 3014

Maslanik, J. A. and Key, J.: On treatments of fetch and stability sensitivity in large-area estimates of sensible heat flux over sea ice, J. Geophys. Res., 100, 4573–4584, doi:10.1029/94JC02204, 1995. 3030

Meier, W. M., Maslanik, J. A., Key, J. R., and Fowler, C. W.: Multiparameter AVHRR-derived products for Arctic climate studies, Earth Int., 1, 5, doi:10.1175/1087-3562(1997)001<0001:MADPFA>2.3.CO;2, 1997. 3014

Onogi, K., Tsutsui, J., Koide, H., Sakamoto, M., Kobayashi, S., Hatsushika, H., Matsumoto, T., Yamazaki, N., Kamahori, H., Takahashi, K., Kadokura, S., Wada, K., Kato, K., Oyama, R., Ose, T., Mannoji, N., and Taira, R.: The JRA-25 Reanalysis, JMSJ, 85, 369–432, doi:10.2151/jmsj.85.369, 2007. 3015

Overland, J. E., McNutt, S. L., Groves, J., Salo, S., Andreas, E. L., and Persson, P. O. G.: Regional sensible and radiative heat flux estimates for the winter Arctic during the surface heat budget of the Arctic Ocean (SHEBA) experiment, J. Geophys. Res., 105, 14093–14102, doi:10.1029/1999JC000010, 2000. 3014

Parkinson, C. L., Rind, D., Healy, R. J., and Martinson, D. G.: The impact of sea ice concentration accuracies on climate model simulations with the GISS GCM, J. Clim., 14, 2606–2623, doi:10.1175/1520-0442(2001)014<2606:TIOSIC>2.0.CO;2, 2001. 3013

TCD
6, 3011–3048, 2012

Persson, P. O. G., Fairall, C. W., Andreas, E. L., Guest, P. S., and Perovich, D. K.: Measurements near the atmospheric surface flux group tower at SHEBA: near-surface conditions and surface energy budget, J. Geophys. Res., 107, 8045, doi:10.1029/2000JC000705, 1992. 3014

Pielke, R. A.: Mesoscale Meteorological Modeling, chap. 7. Parameterization-Averaged Subgrid-Scale Fluxes, Academic Press, 2002. 3019

Raddatz, R. L., Asplin, M. G., Candlish, L., and Barber, D. G.: General characteristics of the atmospheric boundary layer over a flaw lead Polynya region in winter and spring, Bound. Layer Met., 138, 321–335, doi:10.1007/s10546-010-9557-1, 2011. 3020

Rigor, I., Colony, R., and Martin, S.: Variations in surface air temperature observations in the Arctic, 1979–1997, J. Climate, 13, 896–914, doi:10.1175/1520-0442, 2000. 3027

Ruffieux, D., Persson, P. O. G., Fairall, C. W., and Wolfe, D. E.: Ice pack and lead surface energy budgets during LEADEX 1992, J. Geophys. Res., 100, 4593–4612, doi:10.1029/94JC02485, 1995. 3014

Shokr, M. and Kaleschke, L.: Impact of surface conditions on thin sea ice concentration estimate from passive microwave observations, Remote Sens. Environ., 121, 36–50, doi:10.1016/j.rse.2012.01.005, 2012. 3028

Simmonds, I. and Budd, W. F.: A simple parameterization of ice leads in a general circulation model, and the sensitivity of climate to change in Antarctic ice concentration, Ann. Glac., 14, 266–269, 1990. 3013

Spreen, G., Kaleschke, L., and Heygster, G.: Sea ice remote sensing using AMSR-E 89-GHz channels, J. Geophys. Res., 113, C02S03, doi:10.1029/2005JC003384, 2008. 3015, 3028

Tisler, P., Vihma, T., Müller, G., and Brümmer, B.: Modelling of warm-air advection over Arctic sea ice, Tellus A, 60, 775–788, doi:10.3402/tellusa.v60i4.15301, 2008. 3029

Tjernström, M. and Graversen, R. G.: The vertical structure of the lower Arctic troposphere analysed from observations and the ERA-40 reanalysis, Q. J. R. Meteorol. Soc., 135, 431–443, doi:10.1002/qj.380, 2009. 3020

Valkonen, T., Vihma, T., and Doble, M.: Mesoscale modeling of the atmosphere over Antarctic sea ice: a late-autumn case study, Mon. Wea. Rev., 136, 1457–1474, doi:10.1175/2007MWR2242.1, 2008. 3013

Vihma, T., Hartmann, J., and Lüpkes, C.: A case study of an on-ice air flow over the Arctic marginal sea ice zone, Bound. Layer Met., 107, 189–217, doi:10.1023/A:1021599601948, 2003. 3029

TCD
6, 3011–3048, 2012

Vihma, T., Jaagus, J., Jakobson, E., and Palo, T.: Meteorological conditions in the Arctic Ocean in spring and summer 2007 as recorded on the drifting ice station Tara, Geophys. Res. Lett., 35, L18 706, doi:10.1029/2008GL034681, 2008. 3015

von Storch, H. and Zwiers, F. W.: Statistical Analysis in Climate Research, chap. 8 Regression, Cambridge University Press, 1999. 3017, 3018

TCD

6, 3011–3048, 2012

Table 1. Abbreviations used for the different combinations of reanalyses and ice concentration data sets.

Reanalysis	Sensor	Algorithm	Abbreviation
JRA	SSM/I	ASI	JSA
JRA	AMSR-E	ASI	JAA
JRA	AMSR-E	NASA Team 2	JAN
JRA	AMSR-E	Bootstrap	JAB
ERA	SSM/I	ASI	ESA
ERA	AMSR-E	ASI	EAA
ERA	AMSR-E	NASA Team 2	EAN
ERA	AMSR-E	Bootstrap	EAB

TCD
6, 3011–3048, 2012

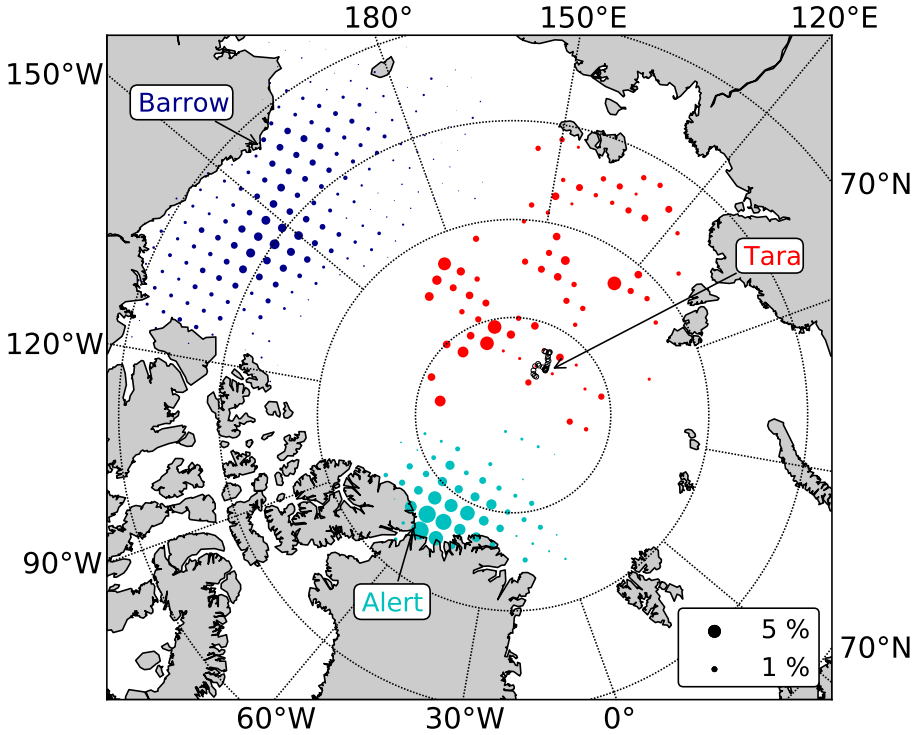

Fig. 1. Distribution of the trajectory starting points upwind of Alert (light blue), Barrow (dark blue) and Tara (red) for JRA and ERA combined. The grid cell size is 100 km and the size of the circles indicates the relative frequency. The arrows mark the in situ stations and the Tara drift track in April 2007.

TCD
6, 3011–3048, 2012

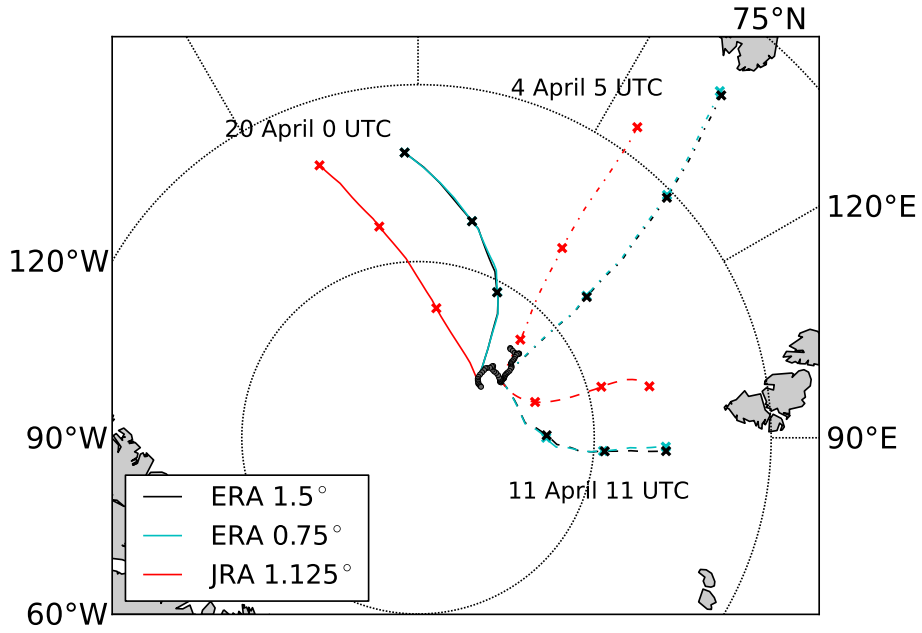

Fig. 2. Three exemplary sets of trajectories arriving at Tara in 2007 caclulated using ERA Interim with two different resolutions and JRA. The differences between crosses are 10 h. The pairs of ERA trajectories are nearly overlapping.

TCD
6, 3011–3048, 2012

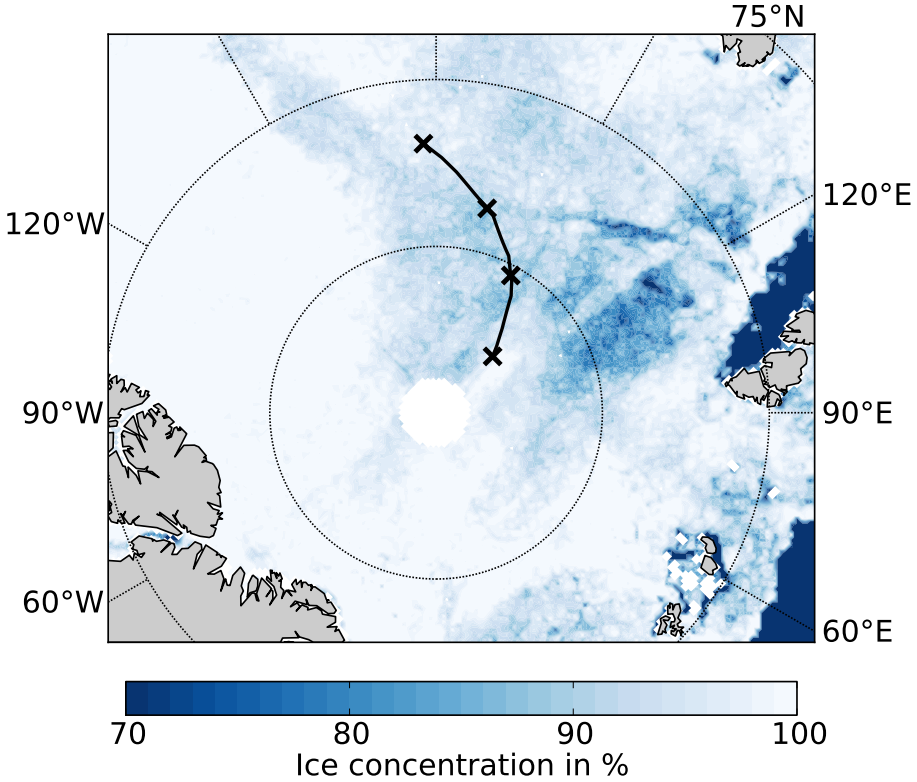

Fig. 3. AA ice concentration on 19 April 2007 and ERA-trajectory from 20 April 2007 00:00 UTC during the last 30 h arriving at Tara (black line).The differences between crosses are 10 h. At this time Tara is located at 87.6° N, 134.9° E.

TCD
6, 3011–3048, 2012

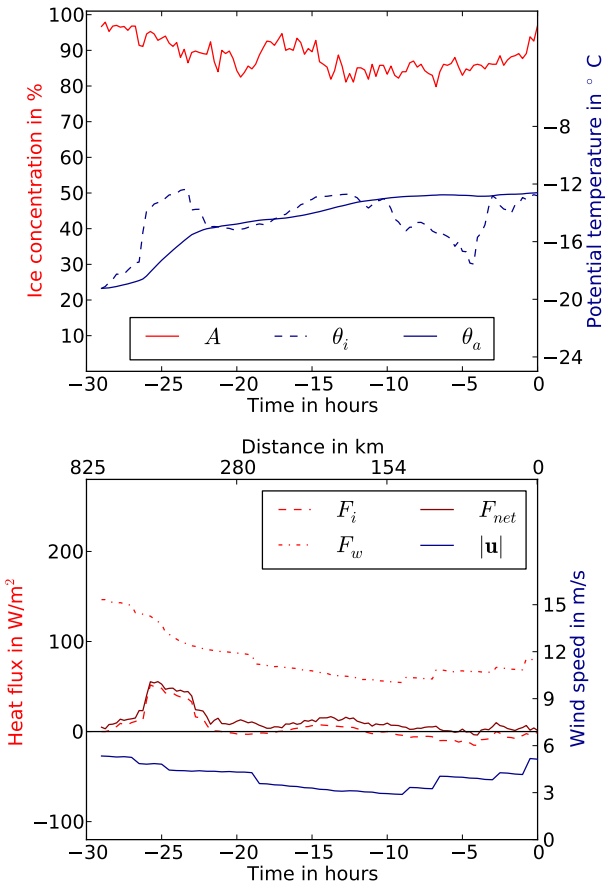

Fig. 4. Time series of the model input and output data on 20 April 2007 00:00 UTC for Tara, AA ice concentration (A), ice surface potential temperature (θ_i), air potential temperature (θ_a), sensible heat flux from ice (F_i), water (F_w) and the resulting net flux (F_{net}), and ERA surface wind speed ($|\boldsymbol{u}|$). The BL depth is 350 m.

TCD
6, 3011–3048, 2012

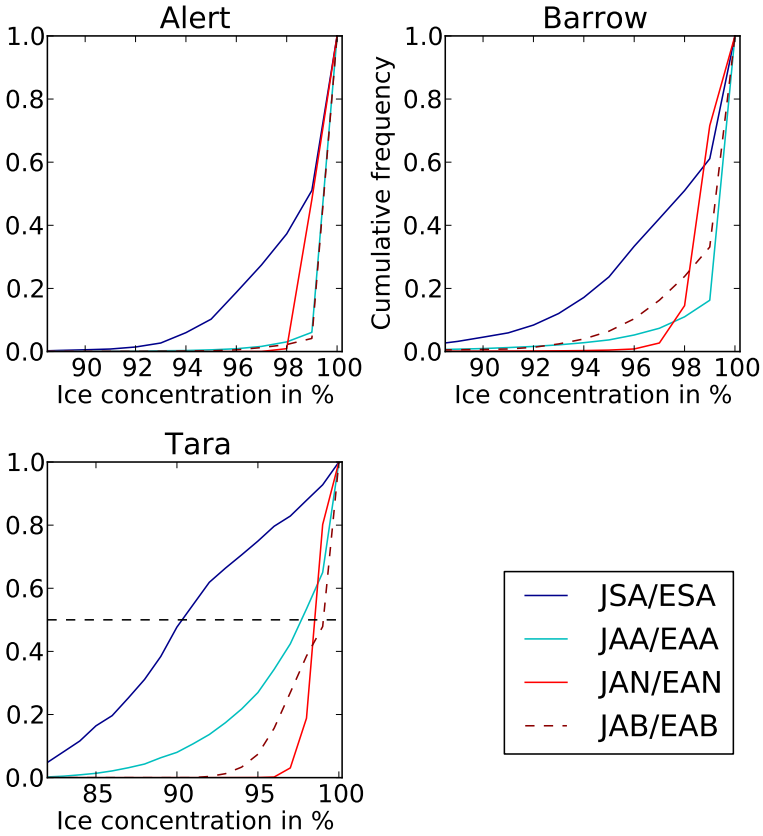

Fig. 5. Cumulative frequency distribution of ice concentrations along the trajectories (ERA and JRA combined) for different ice concentration data sets for Alert, Barrow and Tara.

TCD
6, 3011–3048, 2012

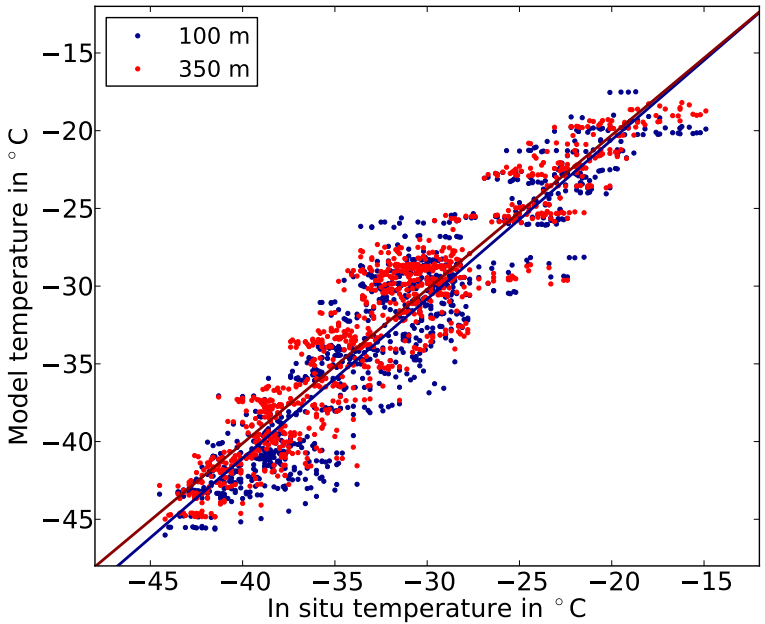

Fig. 6. Scatter plot of in situ and modeled temperatures (AT method) in °C for Alert 2003–2006 for EAA. The colors denote the BL depths and the lines are the corresponding regression lines.

TCD
6, 3011–3048, 2012

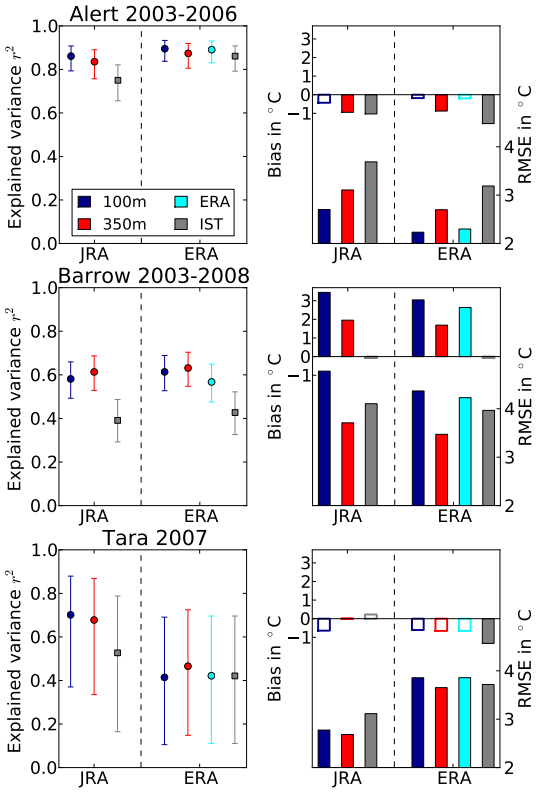

Fig. 7. Explained variances between observed 2-m air temperatures at the stations and modeled temperatures (AT method, colored), as well as mean ice surface temperatures along the trajectories (gray) with 95 % confidence intervals (left), bias and RMSE (right) for Alert (upper), Barrow (middle) and Tara (lower) using AA ice concentrations. The colors denote the BL depths. The blank bars are not significant at the 95 % level.

TCD
6, 3011–3048, 2012

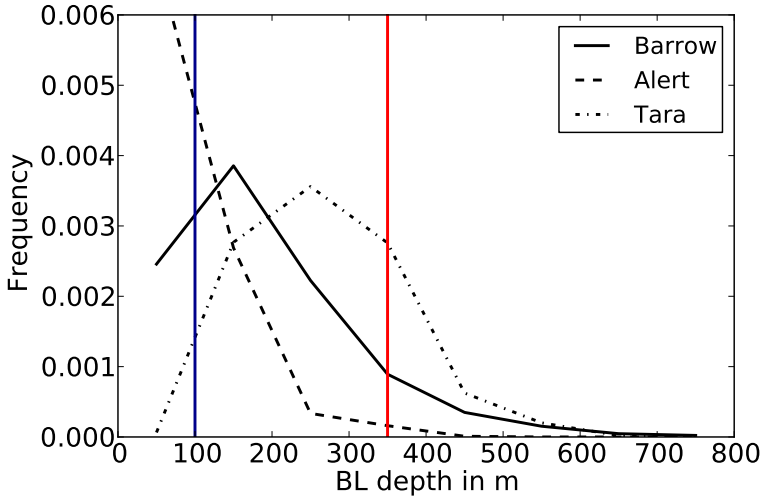

Fig. 8. Frequency distribution of ERA-interim BL depths for Barrow, Alert and Tara. The two constant BL depths which are also used are marked with colors.

TCD
6, 3011–3048, 2012

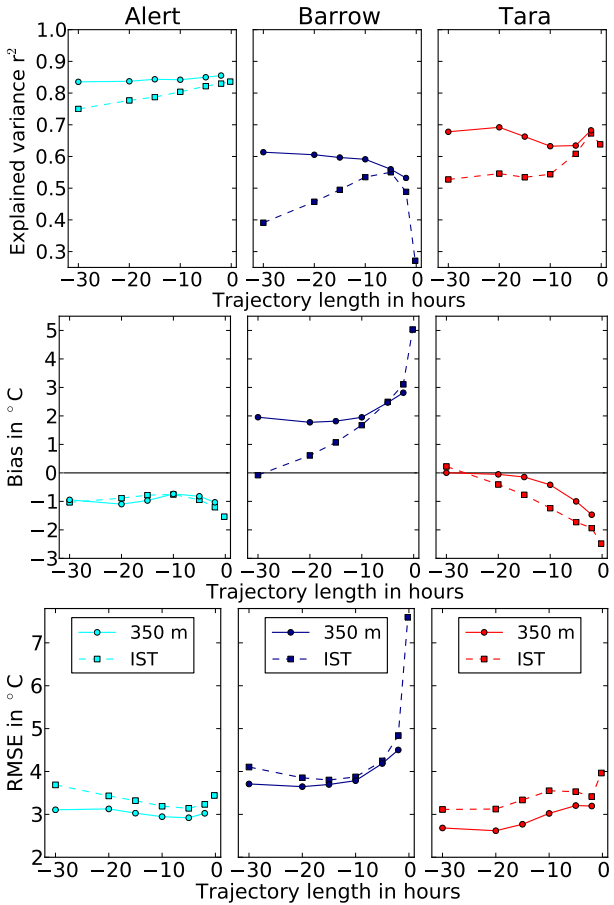

Fig. 9. Explained variances (upper), bias (middle) and RMSE (lower) for Alert, Barrow and Tara (JAA) as a function of trajectory length using the IST and AT methods, with 350 m BL depth in the latter.

TCD
6, 3011–3048, 2012

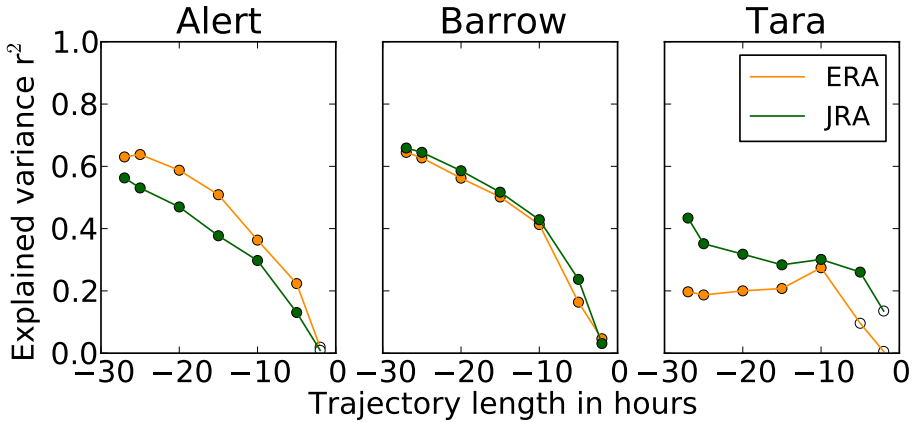

Fig. 10. Explained variances between temperature difference of the model starting temperature and the observed 2-m air temperature at the station and mean sensible heat flux along the trajectories (TV method) for Alert, Barrow and Tara (AA) as a function of trajectory length using a BL depth of 350 m. The filled circles are significant at the 95 % level.

TCD
6, 3011–3048, 2012